Journal of Power Sources 254 (2014) 33–38

Contents lists available at ScienceDirect

Journal of Power Sources

journal homepage: www.elsevier.com/locate/jpowsour

One-dimensional SiOC/C composite nanofibers as binder-free anodes for lithium-ion batteries

Ying Li [a], Yi Hu [b], Yao Lu [a], Shu Zhang [a], Guanjie Xu [a], Kun Fu [a], Shuli Li [a], Chen Chen [a], Lan Zhou [b], Xin Xia [c], Xiangwu Zhang [a,*]

[a] Fiber and Polymer Science Program, Department of Textile Engineering, Chemistry and Science, North Carolina State University, Raleigh, NC 27695-8301, USA
[b] Engineering Research Center for Eco-Dyeing and Finishing of Textiles, Zhejiang Sci-Tech University, Hangzhou, Zhejiang 310018, China
[c] College of Textile and Clothing, Xinjiang University, Urumqi, Xinjiang 830046, China

HIGHLIGHTS

- One-dimensional silicon oxycarbide (SiOC)/C composite nanofibers were fabricated.
- Introducing carbon matrix to SiOC anode can increase the amount of free carbon.
- The capacity of SiOC/C anodes is 70% higher than Si/C anodes after 80 cycles.

ARTICLE INFO

Article history:
Received 27 August 2013
Received in revised form
31 October 2013
Accepted 9 December 2013
Available online 28 December 2013

Keywords:
Polymer derived ceramic
Silicon oxycarbide
Electrospinning
Carbon nanofiber
Lithium-ion battery
Anode

ABSTRACT

One-dimensional silicon oxycarbide (SiOC)/C composite nanofibers were fabricated by electrospinning and subsequent heat treatment. Introducing carbon matrix to SiOC anode material is an efficient way to accommodate the large volume changes during cycling and also increase the amount of free carbon, which is beneficial for improving the reversible capacity. These SiOC/C composite nanofibers form free-standing conductive membranes that can be used directly as battery electrodes without adding carbon black or polymer binder. Results show that after 80 cycles, the discharge capacity of SiOC/C composite nanofiber anodes is 70% higher than that of Si/C nanofiber anodes and more than 1.5 times larger than those of commercial anodes made from graphite. It is, therefore, demonstrated that one-dimensional SiOC/C nanofibers are promising anode material with large capacities and good cycling stability.

© 2013 Elsevier B.V. All rights reserved.

1. Introduction

Lithium-ion batteries (LIBs) as the dominant power sources for portable electronics, electric vehicles and plug-in hybrid electric vehicles have attracted significant attention owing to their ability to offer broad operating temperature range, low self-discharge rate, long cycle life, and no voltage depression [1–5]. Graphite as the commercially-used anode material can only offer a theoretical capacity of 372 mAh g^{-1} [6–8]. Hence, efforts have been put into alternative anode materials [9–11], especially Si-based anode materials due to the extremely large theoretical capacity (3579 mAh g^{-1}) of Si by forming the $Li_{15}Si_4$ phase [12–14]. Numerous studies of high-capacity Si-based anodes have been reported [15–20]. However, the structural failure upon cycling, relatively low conductivity and high cost of Si still hinder its widespread commercial application in practical lithium-ion batteries.

Among other alternative anode materials, polymer-derived ceramics (PDCs) have recently attracted attention [21,22] due to several advantages: 1) they can be easily synthesized; 2) designable physical and chemical properties; 3) excellent mechanical properties; 4) inert to battery components; and 5) low cost. There are mainly two types of PDCs: siloxane-based silicon oxycarbide (SiOC) and silazane-based silicon carbonitride (SiCN). For use in lithium-ion batteries, SiOC generally has higher capacity than SiCN [22–24]. SiOC can be directly made from polysiloxane and consists of Si–O–C glass, free carbon, and micropores, possessing an open

* Corresponding author. Tel.: +1 919 515 6547; fax: +1 919 515 6532.
E-mail addresses: xiangwu_zhang@ncsu.edu, xwzhang01@yahoo.com (X. Zhang).

0378-7753/$ – see front matter © 2013 Elsevier B.V. All rights reserved.
http://dx.doi.org/10.1016/j.jpowsour.2013.12.044

structure of nanodomain molecular network [22,25]. Fig. 1 shows schematically the structure of SiOC material. The Si–O–C glass component can react with lithium reversibly, but the final electrochemical performance of PDC-based anode materials strongly relies on the amount of free carbon [26–28]. In addition, the choices of precursors and experiment conditions are of great importance and have significant effect on the electrochemical performance. Dahn's group has reported more than sixty different SiOC materials [29,30]. However, current SiOC anode materials suffer from large irreversible capacity and poor cyclability [26,29,30].

In this work, we designed one-dimensional SiOC/C composite nanofibers made from electrospun pre-ceramic polymer/polyacrylonitrile (PAN) precursors and sequential thermal treatments in both air and argon environments at high temperatures. Electrospinning as a simple and low-cost method of forming continuous one-dimensional nanofibers could help provide continuous pathways for efficient charge transport along the fiber axis [31–34]. Introducing carbon nanofiber matrix to the SiOC anode material is an efficient way to accommodate the volume changes during cycling and increase the amount of free carbon, which is also beneficial to improve the reversible capacity. These SiOC/C composite nanofibers form free-standing conductive membranes that can be used directly as battery electrodes without adding carbon black or polymer binder. Results indicate that one-dimensional SiOC/C composite nanofiber anodes exhibit excellent electrochemical performance and can be potentially used in next-generation high-energy lithium-ion batteries.

2. Experimental

2.1. Electrode preparation

The pre-ceramic polymer precursor used in this work was 1,3,5,7-tetramethyl-1,3,5,7-tetravinylcyclotertrasiloxane (TTCS, Gelest). Dicumyl peroxide (Acros Organics) was used to promote the crosslinking of TTCS precursor. The chemical structures of TTCS and dicumyl peroxide are shown in Fig. 2. Polyacrylonitrile (PAN, 150,000 g mol^{-1}) obtained from Pfaltz & Bauer Inc was used as carbon precursor. N,N-dimethylformamide (DMF) solvent was purchased from Aldrich. All these reagents were used without further purification.

The preparation of SiOC/C composite nanofibers includes three main steps: 1) crosslinking, 2) electrospinning, and 3) heat treatment (Fig. 3a). In the crosslinking step, the TTCS precursor was heat-treated at 150 °C for 90 min in air with the presence of 1 wt% dicumyl peroxide to form cross-linked TTCS. To obtain small SiOC particle diameter, cross-linked TTCS was crushed by a laboratory blender for 30 min, ball milled for 2 h, and ground in an agate mortar for 30 min, prior to electrospinning. In the electrospinning

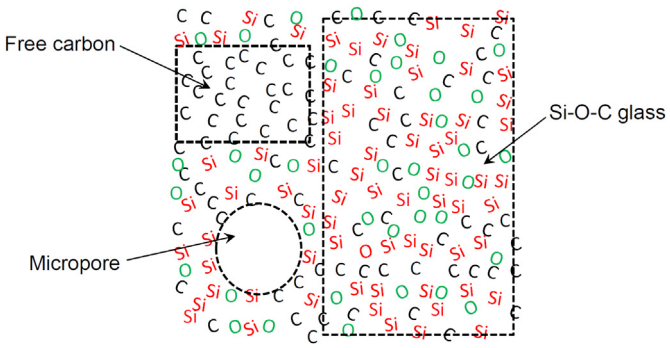

Fig. 1. Schematic structure of SiOC material.

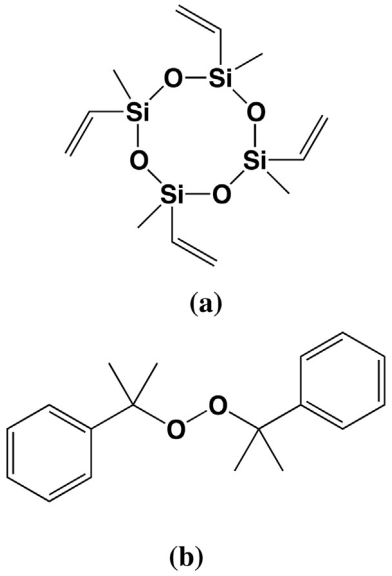

Fig. 2. Chemical structures of (a) TTCS and (b) dicumyl peroxide.

step, 50 wt % cross-linked TTCS was added into an 8 wt% PAN solution in DMF to form a uniform dispersion, which was stirred at 60 °C for 24 h, followed by ultrasonic treatment for 1 h. A variable high voltage power supply (Gamma ES40P–20W/DAM) was used to provide a high voltage (18 kV) for electrospinning. The flow rate used was 0.75 mL h^{-1}, and the needle-to-collector distance was set as 15 cm. Electrospun cross-linked TTCS/PAN fibers were collected on an aluminum foil. In the heat treatment step, electrospun nanofibers were firstly stabilized in air environment at 280 °C for 5 h (heating rate: 5 °C min^{-1}) and then carbonized at 700 °C for 2 h in argon atmosphere (heating rate: 2 °C min^{-1}) to form SiOC/C composite nanofibers. Pure SiOC particles were prepared by employing steps 1 and 3 without conducting the electrospinning process.

For comparison, 10 wt% Si/C composite nanofibers were prepared by replacing cross-linked TTCS with Si nanoparticles (Nanostructured & Amorphous Materials, Inc., 30–50 nm, wt %), but using the same electrospinning and heat treatment conditions. Element analysis results showed that there were around 22.72% Si, 53.91% C and 23.37% other elements like H, N, O, etc., in Si/C composite nanofiber anodes.

2.2. Nanofiber characterization

The morphology of SiOC/C composite nanofibers was examined by field emission scanning electron microscope (FESEM-JEOL 6400F SEM at 5 kV). Energy- dispersive X-ray spectroscopy (EDX) was used to determine the composition of the SiOC/C composite nanofibers. The microstructure of SiOC/C composite nanofibers was observed using transmission electron microscope (Hitachi HF2000 TEM at 200 kV). The structure of composite nanofibers was also investigated by wide-angle X-ray diffraction (WAXD, Rigaku Smartlab). A Nicolet 510P FTIR spectrometer was employed in the range of 4000–400 cm^{-1}, with a resolution of 4 cm^{-1}. For each spectrum, 64 scans were collected. The SiOC/C composite nanofiber mats were directly used for FTIR analysis.

2.3. Electrochemical measurements

SiOC/C composite nanofibers formed free-standing conductive membranes and were used directly as the working electrode in

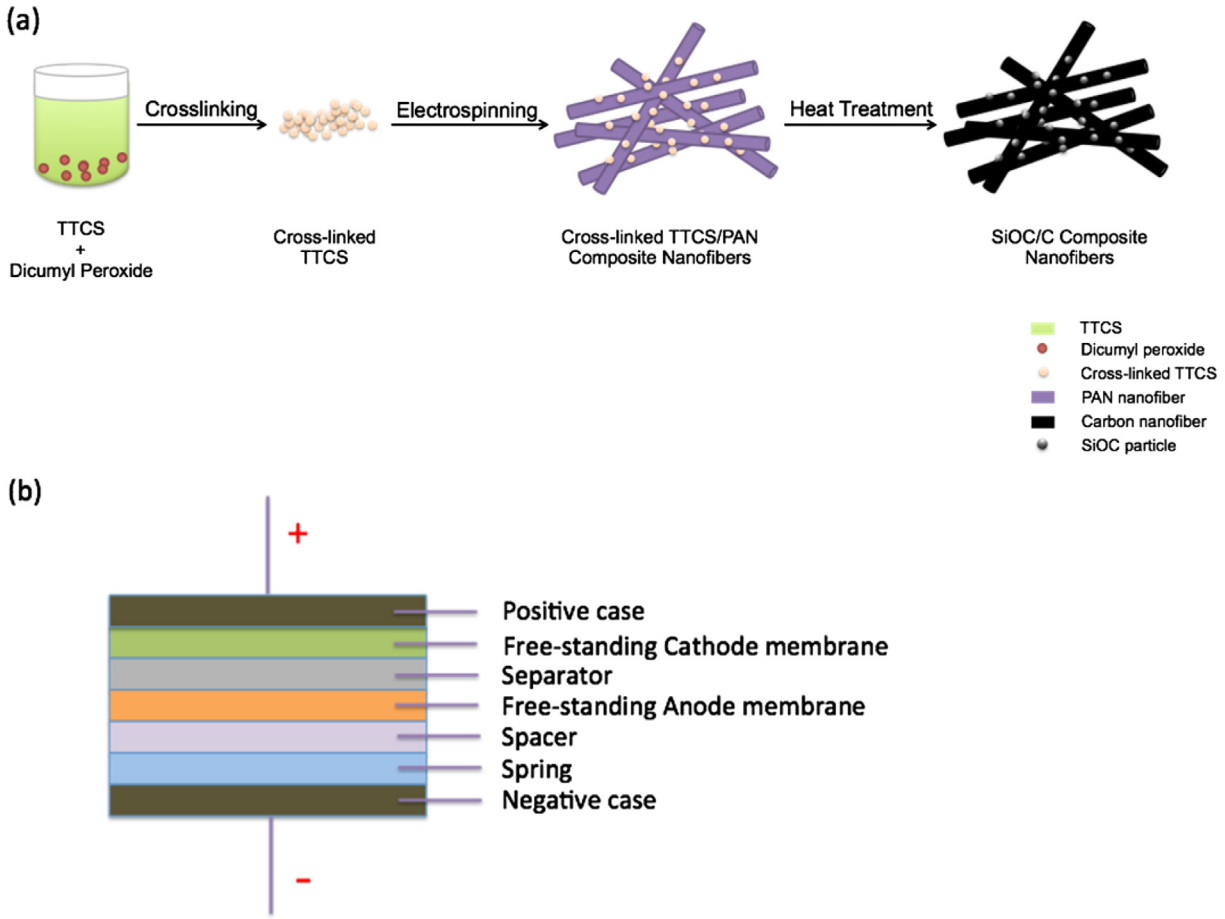

Fig. 3. Schematic of (a) the preparation procedure of SiOC/C composite nanofibers and (b) the corresponding coin cell assembly.

CR2032-type coin cells, as shown in Fig. 3b. The porosity and thickness of the prepared fibrous electrodes were around 50% and 220 μm, respectively. Lithium metal was used as the counter electrode and Celgard 2400 membrane as the separator. The electrolyte used consisted of a 1 mol dm^{-3} solution of $LiPF_6$ dissolved in ethylene carbonate (EC)/diethyl carbonate (DEC)/dimethyl carbonate (DMC) (1/1/1, v/v/v). The electrochemical performance of SiOC/C composite nanofibers was investigated by carrying out galvanostatic charge-discharge experiments at constant current densities of 50 mA g^{-1} between cut-off potentials of 0.01 and 3.0 V. For comparison, the electrochemical performance of Si/C composite nanofibers was also measured using the same experimental conditions.

3. Results and discussion

3.1. Morphology and structure of SiOC/C composite nanofibers

In order to confirm the formation of composite, FTIR spectra of cross-linked pre-ceramic polymer (*i.e.*, cross-linked TTCS), pure SiOC, and SiOC/C composite nanofibers were collected and are shown in Fig. 4. Before crosslinking, the characteristic peaks for TTCS are =C–H stretching and C=C stretching located at 3056 cm^{-1} and 1598 cm^{-1}, respectively [35–37]. As shown in Fig. 4, in the cross-linked TTCS, these two peaks become very weak, indicating the formation of a crosslinking structure. For the cross-linked TTCS, the peaks between 720 and 860 cm^{-1} are assigned to Si–C stretching, and the bands at 1259, 1420, 2904 and 2962 cm^{-1} are assigned to C–H stretching and bending [35–37]. A strong band at 1034–1068 cm^{-1} can be seen from both spectra of cross-linked TTCS and pure SiOC, corresponding to Si–O–Si asymmetric stretching vibrations. After SiOC formation, the C–H bands at 1259 cm^{-1} become weaker while those at 1420, 2904 and 2962 cm^{-1} disappear. A few free –O–H stretching peaks appear at 3500 to 3600 cm^{-1} and the Si–C and Si–O–Si bands at 720 to 860 cm^{-1} and at 1034 to 1068 cm^{-1} become broader, indicating that the open structure of nanodomain molecular network is formed. From Fig. 4, it is also seen that the Si–C and Si–O–Si bands become even weaker and broader after introducing carbon nanofiber matrix.

The morphology of cross-linked TTCS/PAN and SiOC/C composite nanofibers was examined by SEM (Fig. 5). For comparison, SEM images of Si/PAN and Si/C nanofibers are also shown. All nanofibers appear continuous and form 3-D intertwined fibrous

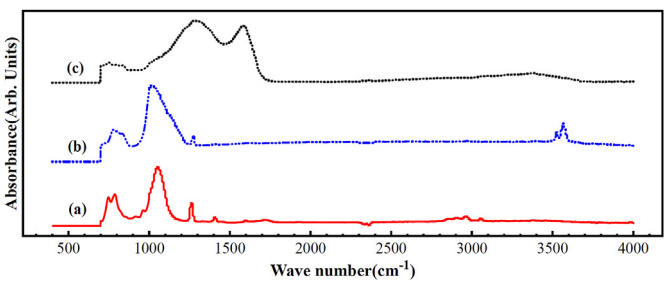

Fig. 4. FTIR spectra of (a) cross-linked TTCS, (b) pure SiOC, (c) SiOC/C composite nanofibers.

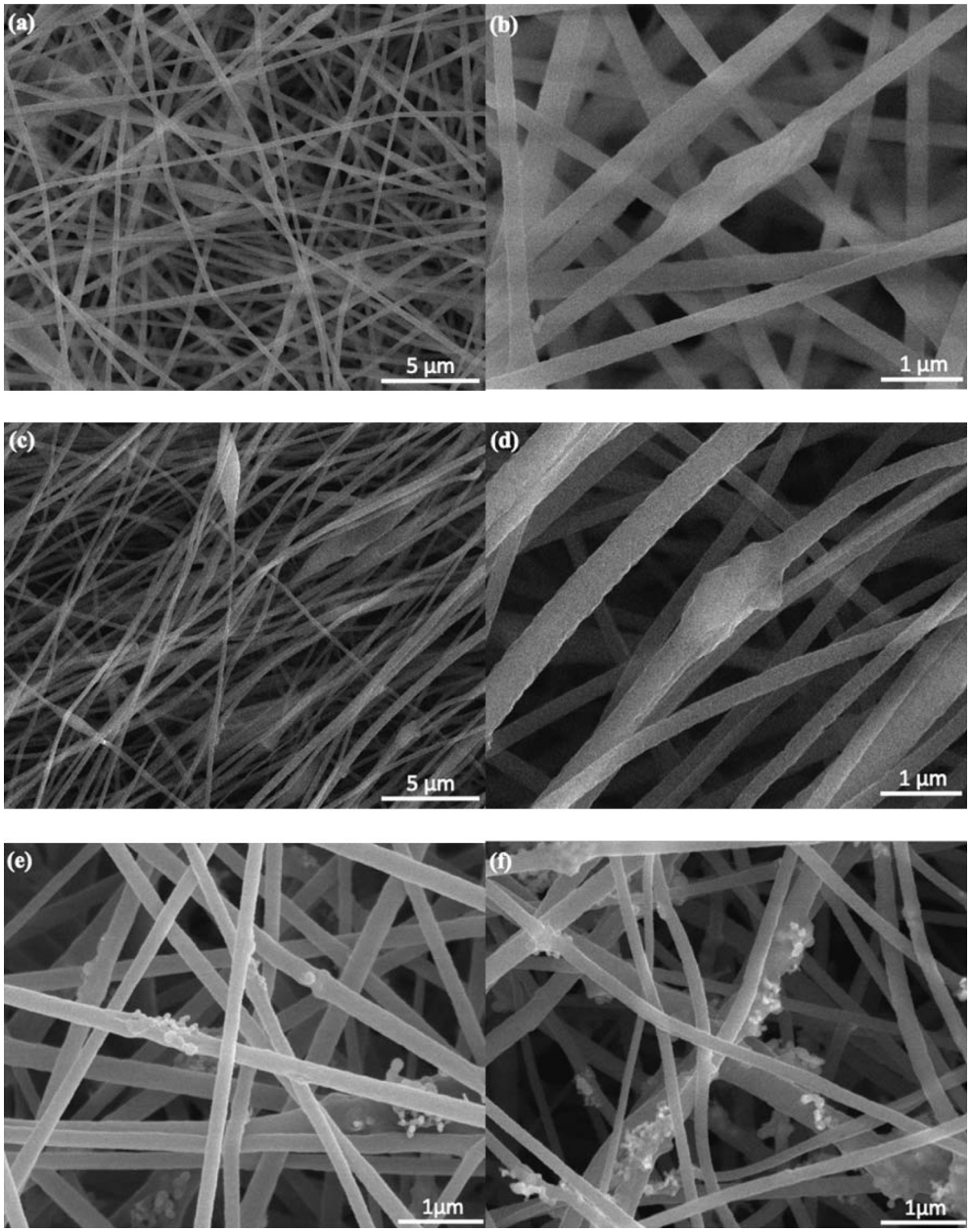

Fig. 5. SEM images of (a,b) cross-linked TTCS/PAN precursor nanofibers, (c,d) SiOC/C composite nanofibers, (e) Si/PAN precursor nanofibers, and (f) Si/C composite nanofibers.

mats. In cross-linked TTCS/PAN precursor nanofibers, the cross-linked TTCS particles are distributed along the fiber axis and some particle clusters can be seen on the fiber surface. After heat treatment, the cross-linked TTCS is converted to electrochemically-active SiOC while PAN precursor is transformed to carbon matrix. Upon pyrolysis, the weight losses of pure PAN and SiOC were around 60% and 10%, respectively. Compared with cross-linked TTCS/PAN precursor nanofibers, the resultant SiOC/C composite nanofibers have slightly smaller diameters, with average fiber diameter decreasing from 350 nm to 300 nm. The SiOC/C composite nanofibers also show less smooth surface and less particle aggregation than Si/C nanofibers. The contents of Si, O and C in SiOC/C composite nanofibers are 10.51, 2.36 and 87.13 wt%, as estimated semi-quantitatively by EDX analysis.

TEM observation provides additional information on the microstructure and distribution of SiOC/C composite nanofibers, as shown in Fig. 6. The carbon nanofiber surface is uneven, which is consistent with the SEM results. In addition, the SiOC particles do not present any ordered structure as confirmed by the selected area electron diffraction (SAED). It can be seen that some SiOC particles are attached on the carbon nanofiber surface and some other particles are embedded inside the carbon nanofiber matrix.

WAXRD measurements were conducted to evaluate the structure evolution of SiOC/C composite nanofibers (Fig. 7). For comparison, the XRD pattern of pure carbon nanofibers and Si/C composite nanofibers are also shown. A weak and broad peak around 25° can be found for all nanofibers due to the formation of carbon nanofiber matrix, showing that the carbon matrix is mainly disordered. The Si/C composite nanofibers show clear peaks at 2θ of 28.4°, 47.4°, 56.2°, 69.2°, 76.5° and 88.1°. In contrast, after incorporating SiOC particles into the carbon matrix, the resultant SiOC/C composite nanofibers exhibit the same pattern as carbon nanofibers, indicating that SiOC particles are basically amorphous, which is in agreement with the TEM analysis.

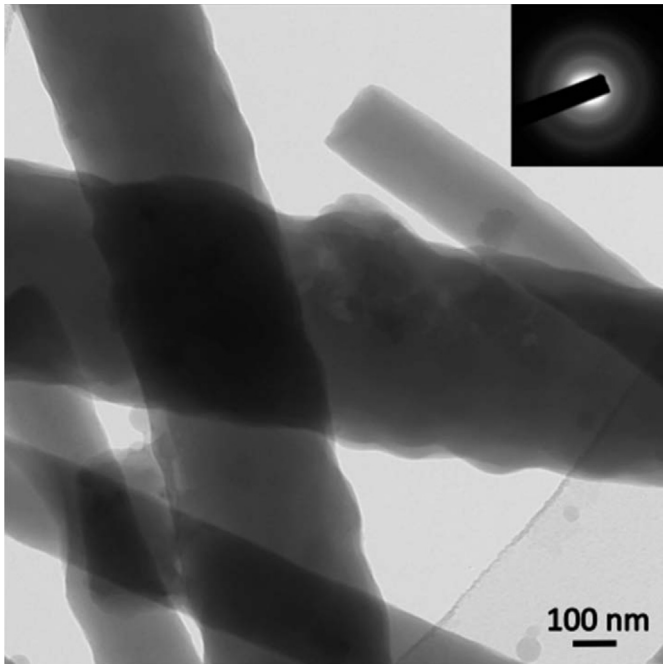

Fig. 6. TEM image of SiOC/C composite nanofibers (SAED pattern, inset).

3.2. Electrochemical performance of PDC/C composite nanofibers

The electrochemical performance of SiOC/C composite nanofibers was investigated by carrying out galvanostatic charge-discharge experiments at a current density of 50 mA g^{-1} between 0.01 and 3.0 V, and the results are shown in Fig. 8. For comparison, the charge–discharge results of Si/C nanofibers are also shown. At the first cycle, the Si/C nanofibers made from Si/PAN precursor show a specific charge capacity of approximately 1334 mAh g^{-1} and discharge capacity of 1026 mAh g^{-1}, respectively, corresponding to a Coulombic efficiency of 76.9%. On the other hand, the specific charge and discharge capacities of SiOC/C composite nanofiber anodes at the first cycle are 1150 and 839 mAh g^{-1}, respectively, corresponding to a Coulombic efficiency of 72.9%.

Fig. 9a and b compare the cycling performance and Coulombic efficiency of Si/C and SiOC/C composite nanofibers. During the first 30 cycles, Si/C composite nanofibers show higher capacities than SiOC/C composite nanofibers. However, the SiOC/C composite nanofibers have a much better cycling stability and exhibit higher capacities after 30 cycles. It is seen that at the 80th cycle, SiOC/C composite nanofibers maintain a high capacity of 669 mAh g^{-1}, while the capacity of Si/C composite nanofibers reduces to 392 mAh g^{-1}. The capacity retention of SiOC/C composite nanofibers at the 80th cycle is 79.7%, which is 70% higher than that (38.2%) of Si/C nanofibers. From Fig. 9b, it is seen that after 10 cycles, the Coulombic efficiency of SiOC/C composite nanofiber anodes are more than 99%, which is higher than that (~97.5%) of Si/C composite nanofibers. For comparison, the cycling performance and Coulombic efficiency of pure SiOC powder are also shown in Fig. 9c. It can be seen that at the first cycle, the pure SiOC powder

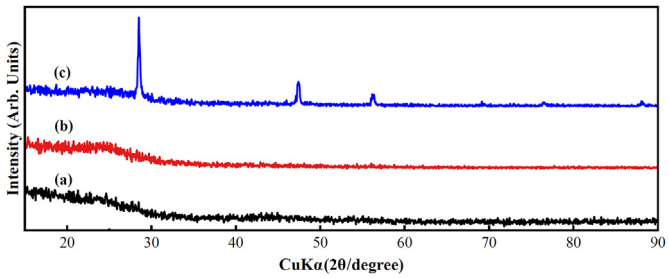

Fig. 7. XRD patterns of (a) carbon nanofibers, (b) SiOC/C composite nanofibers, and (c) Si/C composite nanofibers.

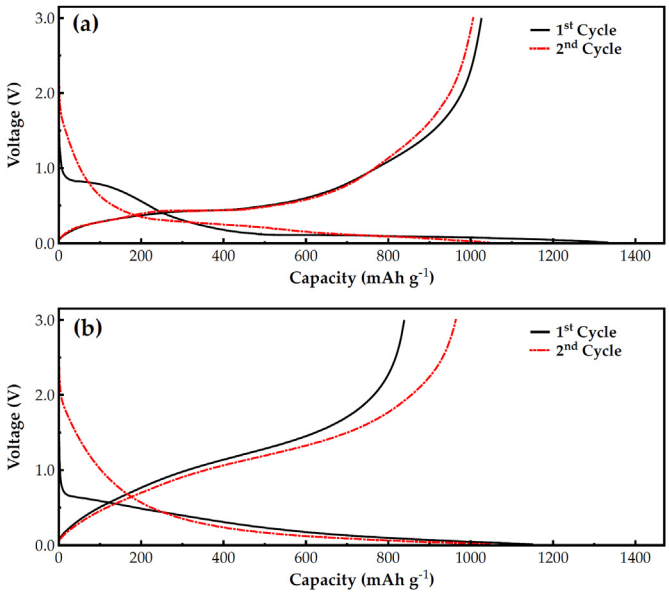

Fig. 8. Galvanostatic charge–discharge curves of (a) Si/C and (b) SiOC/C composite nanofibers.

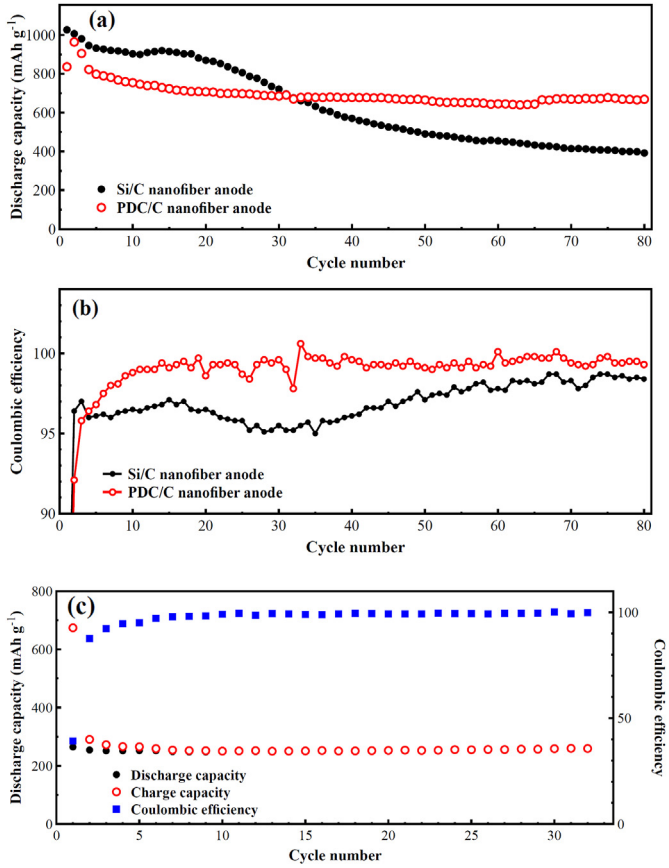

Fig. 9. Cycling performance comparison of (a) Si/C composite nanofibers, (b) SiOC/C composite nanofibers and (c) pure SiOC powder.

shows a charge capacity of approximately 674 mAh g^{-1} and discharge capacity of 264 mAh g^{-1}, respectively, corresponding to a Coulombic efficiency of 39.2%. The comparison of pure SiOC powder with Si/C and SiOC/C composite nanofibers indicates that introducing one-dimensional carbon nanofiber matrix to the SiOC anode material is an efficient way to improve the reversible capacity.

These results demonstrate that one-dimensional SiOC/C composite nanofibers have more stable cycling performance than Si/C composite nanofibers. The enhanced cycling performance is mainly due to the introduced free carbon and carbon-rich phase, which could increase lithium storage sites. The free carbon phase is typically a mixture of disordered carbon, nano-crystalline graphite and graphene layers [26,27]. As increase in free carbon content, the size of nanodomains may decrease, which is beneficial for improving the electrochemical performance [25]. The unique morphology and structure of the one-dimensional conductive nanofibrous structure can also enhance the electrochemical behavior of SiOC/C composite nanofibers. The presence of free space around the entangled SiOC/C composite nanofibers allows the formation of a porous network through which Li^+ ions can migrate easily and reach all SiOC/C composite nanofiber surfaces. These factors may contribute to the high reversible capacity and good cycling performance of SiOC/C composite nanofibers.

4. Conclusions

In this work, we designed one-dimensional SiOC/C composite nanofibers made from electrospun pre-ceramic polymer/PAN precursors and sequential thermal treatments in both air and argon environments at high temperatures. The introduced free carbon and carbon-rich phase increase lithium storage sites, resulting in excellent electrochemical performance. Used as the anode in lithium-ion half cells, the initial discharge capacity of SiOC/C composite nanofibers is 839 mAh g^{-1}. After 80 cycles, the discharge capacity of SiOC/C composite nanofibers is still 669 mAh g^{-1}, which is 70% higher than that of Si/C nanofiber anodes and more than 1.5 times larger than those of commercial anodes made from graphite. Results indicated that preparing one-dimensional SiOC/C composite nanofibers via electrospinning is a simple, effective and low-cost way to achieve excellent electrochemical performance for high-capacity lithium-ion battery anodes.

Acknowledgments

This research was supported U.S. Department of Energy under Grant No: DE-EE0001177, Advanced Transportation Energy Center, ERC Program of the National Science Foundation under Award Number EEC-08212121, Open Foundation of Top Academic Discipline of Applied Chemistry and Eco-Dyeing & Finishing Engineering of Textiles of Zhejiang Province, and Zhejiang Provincial Natural Science Foundation under Award Number LY12E03005.

References

[1] Z. Yang, J. Zhang, M.C.W. Kintner-Meyer, X. Lu, D. Choi, J.P. Lemmon, J. Liu, Chem. Rev. 111 (2011) 3577.
[2] B. Dunn, H. Kamath, J.M. Tarascon, Science 334 (2011) 928.
[3] J.M. Tarascon, Philos. Trans. R. Soc. A 368 (2010) 3227.
[4] J.M. Tarascon, M. Armand, Nature 414 (2001) 359.
[5] M. Armand, J.M. Tarascon, Nature 451 (2008) 652.
[6] D. Aurbach, E. Zinigrad, Y. Cohen, H. Teller, Solid State Ionics 148 (2002) 405.
[7] M. Alcoutlabi, J. Liwen, B. Guo, S. Li, Y. Li, S. Zhang, O. Toprakci, X. Zhang, AATCC Rev.: Mag. Text. Dyeing, Print. Finish. Ind. 11 (2011) 45.
[8] H. Shi, J. Power Sources 75 (1998) 64.
[9] C.A. Bonino, L. Ji, Z. Lin, O. Toprakci, X. Zhang, S.A. Khan, ACS Appl. Mater. Interfaces 3 (2011) 2534.
[10] Z. Lin, L. Ji, M.D. Woodroof, X. Zhang, J. Power Sources 195 (2010) 5025.
[11] L. Ji, O. Toprakci, M. Alcoutlabi, Y. Yao, Y. Li, S. Zhang, B. Guo, Z. Lin, X. Zhang, ACS Appl. Mater. Interfaces 4 (2012) 2672.
[12] M.N. Obrovac, L. Christensen, Electrochem. Solid-State Lett. 7 (2004) A93.
[13] M.N. Obrovac, L.J. Krause, J. Electrochem. Soc. 154 (2007) A103.
[14] J. Li, J.R. Dahn, J. Electrochem. Soc. 154 (2007) A156.
[15] M.D. Fleischauer, M.N. Obrovac, J.R. Dahn, J. Electrochem. Soc. 155 (2008) A851.
[16] L. Ji, K.-H. Jung, A.J. Medford, X. Zhang, J. Mater. Chem. 19 (2009) 4992.
[17] P.R. Abel, Y.-M. Lin, H. Celio, A. Heller, C.B. Mullins, ACS Nano 6 (2012) 2506.
[18] Y. Li, G. Xu, L. Xue, S. Zhang, Y. Yao, Y. Lu, O. Toprakci, X. Zhang, J. Electrochem. Soc. 160 (2013) A528.
[19] C.K. Chan, H. Peng, G. Liu, K. McIlwrath, X.F. Zhang, R.A. Huggins, Y. Cui, Nat. Nanotechnol. 3 (2007) 31.
[20] J. Yang, S.T. John, J. Mater. Chem. A 1 (2013) 7782.
[21] H. Bréquel, J. Parmentier, S. Walter, R. Badheka, G. Trimmel, S. Masse, J. Latournerie, P. Dempsey, C. Turquat, A. Desmartin-Chomel, L. Le Neindre-Prum, U.A. Jayasooriya, D. Hourlier, H.J. Kleebe, G.D. Sorarù, S. Enzo, F. Babonneau, Chem. Mater. 16 (2004) 2585.
[22] M. Graczyk-Zajac, C. Fasel, R. Riedel, J. Power Sources 196 (2011) 6412.
[23] Y. Feng, Electrochim. Acta 55 (2010) 5860.
[24] J. Shen, R. Raj, J. Power Sources 196 (2011) 5945.
[25] A. Saha, R. Raj, D.L. Williamson, J. Am. Ceram. Soc. 89 (2006) 2188.
[26] M. Graczyk-Zajac, L. Toma, C. Fasel, R. Riedel, Solid State Ionics 225 (2012) 522.
[27] J. Kaspar, M. Graczyk-Zajac, R. Riedel, Solid State Ionics 225 (2012) 527.
[28] E. Erdem, V. Mass, A. Gembus, A. Schulz, V. Liebau-Kunzmann, C. Fasel, R. Riedel, R.-A. Eichel, Phys. Chem. Chem. Phys. 11 (2009) 5628.
[29] W. Xing, J. Electrochem. Soc. 144 (1997) 2410.
[30] A.M. Wilson, J.N. Reimers, E.W. Fuller, J.R. Dahn, Solid State Ionics 74 (1994) 249.
[31] L. Ji, Y. Yao, O. Toprakci, Z. Lin, Y. Liang, Q. Shi, A.J. Medford, C.R. Millns, X. Zhang, J. Power Sources 195 (2010) 2050.
[32] Y. Li, B. Guo, L. Ji, Z. Lin, G. Xu, Y. Liang, S. Zhang, O. Toprakci, Y. Hu, M. Alcoutlabi, Carbon 51 (2013) 185.
[33] L. Ji, Z. Lin, R. Zhou, Q. Shi, O. Toprakci, A.J. Medford, C.R. Millns, X. Zhang, Electrochim. Acta 55 (2010) 1605.
[34] Y. Liang, L. Ji, B. Guo, Z. Lin, Y. Yao, Y. Li, M. Alcoutlabi, Y. Qiu, X. Zhang, J. Power Sources 196 (2011) 436.
[35] A. Nyczyk, C. Paluszkiewicz, A. Pyda, M. Hasik, Spectrochim. Acta Part A 79 (2011) 801.
[36] A.L. Smith, Spectrochim. Acta 16 (1960) 87.
[37] J. Gnado, P. Dhamelincourt, J. Raman Spectrosc. 24 (2005) 63.